A DISTORTION EVALUATION FRAMEWORK IN 3D VIDEO VIEW SYNTHESIS

Andrei I. Purica[⋆†]*, Marco Cagnazzo*[⋆]*, Beatrice Pesquet-Popescu*[⋆]*, Frederic Dufaux*[⋆]*, Bogdan Ionescu*[†]

[⋆]LTCI, CNRS, Télécom ParisTech, Université Paris-Saclay, 75013, Paris, France
[†]University Politehnica of Bucharest,061071, Romania
Email:{purica, cagnazzo, pesquet, dufaux }@telecom-paristech.fr, bionescu@imag.pub.ro

ABSTRACT

Demand for 3D content increased over the last years and more attention was dedicated to methods used in 3D content creation and transmission. View synthesis methods introduce localized artifacts when creating new virtual views. Evaluating these methods require therefore a different approach, in order to identify and emphasize synthesis artifact prone areas, while diminishing the impact, of other types of artifacts, such as those produced by quantization during the video coding. In this paper, we propose an artifact evaluation technique which was shown to provide a better differentiation of synthesis methods, while additional information can be extrapolated from the results about the spatial localization of typical synthesis artifacts and their impact on overall image quality.

***Index Terms*—** View Synthesis, Visual quality assessment, Multi-View Video, SSIM, Depth-Image-Based-Rendering

1. INTRODUCTION

3D content has become widespread in the past years. Technology advancements in display, transmission and encoding fields allow 3D to be used in common everyday applications. Some of the typical usage scenarios involve immersive teleconference systems, free view point television (FTV) [1], medical applications, gaming and entertainment [2].

Due to the high quantity of information contained in 3D data, new encoding and compression methods are required. Several formats exists for storing 3D video data. Some of the most commonly used are stereo video, MultiView Video and Multiview-Video-plus-Depth (MVD) [3]. MVV format is comprised of a set of N video sequences, representing the same scene and acquired simultaneously by a system of N cameras, in different spatial configurations. Most commonly, a parallel camera line is used. MVD format is similar with MVV, but, in addition to texture, it also stores depth information associated with each video sequence. This approach provides more flexibility, as depth maps can be used to more efficiently render additional video sequences from virtual points of view, using methods like Depth-Image-Based-Rendering (DIBR) [4].

View synthesis is the process of extrapolating or interpolating a view from available views. Numerous methods have been developed in this field. View synthesis techniques can be mainly classified in three categories [5]. Methods in the first category, such as DIBR, use explicit geometry information to warp pixels from the original view to their correct positions in the virtual view [6] [7]. Methods in the second category rely only on implicit geometry, for example pixel correspondences which can be computed using methods such as optical flow [8] [9]. Finally, methods in the third category use filtering and interpolation to synthesize the view. Examples include light field rendering [10], concentric mosaics [11] or lumigraph [12].

The Moving Picture Experts Group (MPEG), expressed interest in MVD formats for their ability to support 3D video applications. The idea was to develop a 3D extension of the High Efficiency Video Coding (HEVC) standard [13]. An experimental framework was developed to conduct experiments [14] with 3D video. A 3D-HEVC test model (3D-HTM) [15] was also created, which includes the View Synthesis Reference Software 1DFast (VSRS-1DFast) designed for parallel camera systems.

Some of the main issues in view synthesis are caused by areas which are hidden in the original view (e.g., and i.e., background covered by foreground objects) but become visible when changing the point of view. These areas are referred to as disocclusions, and in the synthesized views they produce holes in the image. Traditionally, this problem is fixed using inpainting [16] [17] [18]. However, different techniques can be used that exploit the temporal correlations in a video sequence. The scene background can be extracted from multiple time instances of the video sequence, and used to fill the disoccluded areas [19] [20]. Temporal correlations can also be used. The authors in [21] compute motion vector fields in the rendered view to improve the synthesis. In [22] the authors use block-based motion estimation in the reference views, and retrieve information about disoccluded areas by warping the start and end point of the motion vectors.

[†]Part of this work was supported under ESF InnoRESEARCH POSDRU/159/1.5/S/132395 (2014-2015).

[⋆]Part of this work was supported under CSOSG, ANR-13-SECU-0003, SUrveillance de Reseaux et d'InfrastruCtures par des systemes AeroporTes Endurants (SURICATE) (2013-2016).

Other sources of errors in view synthesis are related to the quality of depth maps. While artificially generated sequences have almost ideal depth maps, real sequences will have distortions and errors in the depth maps, due to the limitation of the recording devices. Low quality depth maps lead to distortions of foreground object and larger or incorrect holes (e.g. new holes might be generated and existing holes may be covered incorrectly during the warping process) in the synthesized views. Most synthesis methods, preferably, use two reference views, a left and right one with respect to the virtual view position. This is favored in order to avoid border disocclusions [23]. Another issue is the texture-depth alignment, which may lead to a missmatch of the left and right warping of the reference views. Other methods, such as [24] or [25], preprocess the depth maps, with the goal of providing a better foreground-background transition. In [26], a rendering technique is presented based on a background-foreground separation filtering step.

In addition to errors caused by the actual warping process, all synthesized views are also affected by the encoding quality of the reference views or depth maps. When using encoded reference views, the pixels that are warped in the synthesized view are subject to an absolute quantization error of up to half the quantization step. Encoded depth maps will also be subjected to quantization errors, especially since they are usually encoded using higher QPs. However, the quantization errors in depth maps will impact the synthesized view in a different manner. A small error in the depth map, results in warping the pixel to a slightly different position in the virtual view. While this is not a big issue for pixels located in areas with uniform texture, it can create very high distortions on the edges of objects (consider a scene with a black object on white background). Finally, another source of errors for depth maps is the quantization of real depth values to, usually, 256 levels.

Because of the multiple sources of errors which are usually notuniformly spread across the image, unlike encoding errors, evaluating the quality of a synthesized image is not a trivial problem. Measures such as Peak-Signal-to-Noise-Ratio (PSNR) provide a good objective evaluation but fail to emphasize the errors caused by object distortions. Evaluation methods that take into account the structure of the image were created, one of the most popular being the structural similarity based metric (SSIM) [27] (see Sec. 3.1). While SSIM takes into account the structural distortions of an image, small differences in background color reproduction might mask the impact of important artifacts. As discussed above, the majority of high errors in view synthesis are mostly located close to the edges of foreground objects. In this paper we propose a new view synthesis evaluation technique, based on SSIM, which focuses on comparing view synthesis artifacts around sensible, error prone, areas of the image. Two different methods are used for selecting the areas of interest in the evaluation. Firstly, we analyze the distribution of errors and separate high synthesis errors from quantization ones. A second approach is focused on directly evaluating the areas predicted differently by the two tested methods. We show this technique to bring a better differentiation of synthesis methods with respect to the impact of synthesis artifacts on the image quality. Also, additional information can be extrapolated on the spatial localization of distortions when compared to an SSIM or PSNR evaluation.

The rest of this paper is organized as follows. The next section presents the view synthesis methods used for evaluation. In Sec. 3 we describe the proposed evaluation technique. In Sec. 4 we show the results we obtained and Sec. 5 concludes the paper.

2. VIEW SYNTHESIS METHODS

We evaluate three different view synthesis methods. The DIBR implementation of VSRS-1DFast [15], a method that uses a filtering technique described in [26] and a method that blends temporal prediction with DIBR synthesis [28].

All methods use depth maps to compute disparity. Usually, depth maps are given with inversed quantized values between $[0 \quad 255]$. When dealing with 1D camera systems, disparity only has an x component which can be computed from the depth maps of the reference views as [2]:

$$\mathbf{d}(\mathbf{k}) = f \cdot B \left[\frac{Z(\mathbf{k})}{255} \left(\frac{1}{Z_{min}} - \frac{1}{Z_{max}} \right) + \frac{1}{Z_{max}} \right] \qquad (1)$$

where Z is the inverse quantized depth, Z_{min} and Z_{max} are the minimum and maximum depth values respectively, B is the baseline (i.e. the distance between the synthesized view and base one) and f is the focal length of the camera.

The first method (VSRS-1DFast) uses two or three texture and depth views and synthesizes any number of intermediary views. This method can work with sub-pixel precision up to a factor of four. The warping, interpolation and hole filling are carried out line-wise. Two reliability maps are used to mark disoccluded areas for filling. And a similarity enhancement step adapts the histograms of the left and right warped views. The two warped images, from left and right base views, can be either combined, or the disocclusions in one image can be filled using the other one.

The filtering method presented in [26] uses an additional intermediary step to perform a filtering of the combined, upsampled, warped images in order to perform a foreground background separation and interpolation.

The method in [28] uses temporal correlations to produce multiple predictions of a synthesized frame from different time instants and uses an adaptive blending method to combine the temporal and inter-view predictions. The motion vector fields (MVF) in the synthesized view ($\mathbf{v}_s$) are obtained by imposing an epipolar constraint between the MVF in the reference view ($\mathbf{v}_r$) and the disparity fields at two time instants ($\mathbf{d}_{t\_}$ and $\mathbf{d}_t$) as shown in Eq. 2:

$$\mathbf{v}_s(\mathbf{k} + \mathbf{d}_t(\mathbf{k})) = \mathbf{v}_r(\mathbf{k}) + \mathbf{d}_{t\_}(\mathbf{k} + \mathbf{v}_r(\mathbf{k})) - \mathbf{d}_t(\mathbf{k}) \qquad (2)$$

where $\mathbf{k} = (x, y)$ is a position in the image. Using a future and a past reference frame for motion estimation in each base view allows the computation of four MVFs. Thus, four temporal predictions and two inter-view predictions are obtained. An adaptive blending method reduces the motion estimation errors by using only inter-view prediction for these areas.

3. PROPOSED SYNTHESIS EVALUATION

As discussed in Sec. 1, view synthesis methods should be evaluated not only with respect to PSNR, but also with respect to a metric that takes into account the structure of the image, like SSIM. However the main issues in synthesis are the disoccluded areas and the distortion of foreground object and other artifacts caused by texture-depth misalignment or imprecise depth maps. Thus, when comparing different methods, areas around foreground object edges and disocclusions should be emphasized in the evaluation. Smooth background areas typically have low errors (see Sec. 4). It is reasonable to assume that methods which bring only small corrections in these areas will not have a visual impact even though PSNR gains can be achieved. In what follows, we will describe the SSIM metric and show how a selection of artifact prone areas can be achieved for better evaluating view synthesis methods.

3.1. Structural Similarity index (SSIM)

In [27], Wang *et al.* assume that the human visual system is highly focused on the perception of structural information of a scene. The proposed measure is designed to asses the degradation of structural information. SSIM separates the similarity measurement in three components: luminance, contrast and structure. A condensed form of the SSIM is given by:

$$SSIM(r, d) = \frac{(2\mu_r\mu_d + C_1)(2\sigma_{rd} + C_2)}{(\mu_r^2 + \mu_d^2 + C_1)(\sigma_r^2 + \sigma_d^2 + C_2)} \quad (3)$$

where, r and d refer to windows in the reference and distorted images, μ_r and μ_d are the means of r and d, σ_r and σ_d are the standard deviations and σ_{rd} is the correlation coefficient between r and d. C_1 and C_2 are two variables used to stabilize the division with weak denominator. The score of an image can then be obtained by centering the windows in each pixel and averaging the SSIM index, this is known as mean SSIM (MSSIM).

3.2. Histogram based area selection

When testing two view synthesis methods, a first way of selecting the areas prone to synthesis errors would be to look for pixels which have a relative high absolute error. This can provide a good indication on the quality of the synthesis methods. Errors produced by the quantization during the encoding of the reference views and errors caused by depth quantization or interpolation process are usually uniformly spread and do not necessarily depend on the structure of the scene or the view synthesis method employed. This can also be observed in Fig. 1 where two binary masks are shown. Black indicates pixels that have an absolute error larger than twice the mean absolute error.Fig. 1(a) shows the mask for a frame encoded with 3D-HEVC at QP 25 and Fig. 1(b) is obtained from the same frame synthesized with VSRS-1DFast from non-encoded reference views. It is easily noticeable that in the case of encoding, high errors are spread across the image. In the case of synthesis, impactful errors are concentrated and their spatial positioning is dependent on the structure of the scene. Focusing the synthesis evaluation on these areas can provide a better indication of the methods quality for object distortion, while ignoring other less impactful error sources, like quantization errors produced by encoding.

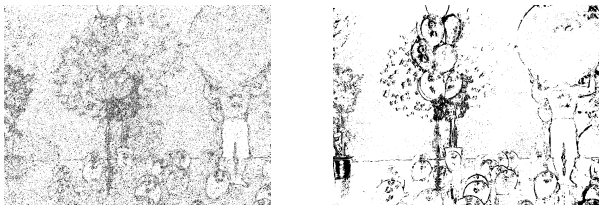

(a) 3D-HEVC encoding (b) Synthesis

Fig. 1. Binary masks on Balloons sequence frame 1, black indicates pixels with high absolute errors. 1(a) was obtained from a 3D-HEVC encoding at QP 25 and 1(b) from the same view synthesized from non-encoded reference views.

The threshold used in generating the mask should be selected in such a way that is able to separate the large errors coming from synthesis. In order to do this, we depict the distribution of absolute errors for a synthesized view. In Fig. 2, as expected, we find a large percentage of pixels with small errors, this is normal for encoded sequences as errors are normally distributed around zero. However, in Fig. 2 we find an increased error density around a larger value, marked with a red line in the figure. This is caused by the synthesis process. As discussed, the synthesis will introduce high distortions compared to the quantization errors especially for low QPs. Quantization errors are bounded in absolute value by half the quantization interval, while synthesis errors can be made higher. The threshold can be determined by finding this value where higher errors are concentrated.

Let us consider two vectors $\mathcal{E} = [\epsilon_1, \epsilon_2, .., \epsilon_n]$ and $\mathbf{P} = [p_1, p_2, .., p_n]$. $\mathcal{E}$ contains absolute error values such that $\epsilon_x > \epsilon_{x+1}$ and $\epsilon_x - \epsilon_{x+1} = constant$. $\mathbf{P}$ is the percentage of pixels with an absolute error between ϵ_x and ϵ_{x+1}. The threshold can be expressed as:

$$\mathcal{T} = \mathcal{E}(\min(\{x|\Delta(x) > 0\}) + 1) \quad (4)$$

where $\Delta(x)$ is:

$$\Delta(x) = p_{x+1} - p_x \quad (5)$$

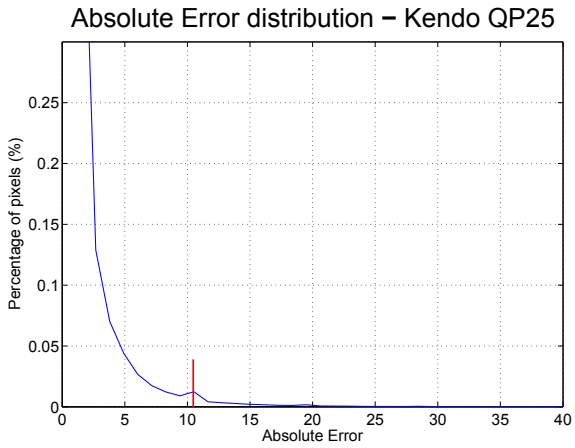

Fig. 2. Absolute error distribution for a synthesized frame in Kendo sequence, at QP=25.

The binary mask used for synthesis distorted area selection can then be computed as:

$$B(x,y) = \begin{cases} 0 & \text{if } \mid (I_r(x,y) - I_d(x,y)) \mid < \mathcal{T} \\ 1 & \text{if } \mid (I_r(x,y) - I_d(x,y)) \mid \geq \mathcal{T} \end{cases} \quad (6)$$

where I_r and I_d are the reference and distorted images.

However, this approach can produce different masks for two evaluated synthesis methods (B_{d_1} and B_{d_2}). In order to assure a consistent evaluation in both compared methods, the SSIM index should be computed using a single mask. This can be achieved by performing the evaluation in the locations obtained by merging the two masks as shown in Eq. 7.

$$B_{hist}(x,y) = B_{d_1}(x,y) \vee B_{d_2} \quad (7)$$

where $\vee$ is the logical *or* operation.

The score of each method can then be obtained by averaging the SSIM index over all pixels selected with the binary mask:

$$SSIM^{d1}_{hist}(I_r, I_{d_1}, I_{d_2}) = \frac{1}{\sum_{x=1}^{M}\sum_{y=1}^{N} B_{hist}(x,y)} \sum_{x=1}^{M}\sum_{y=1}^{N} SSIM(r(x,y), d1(x,y)) \times B_{hist}(x,y) \quad (8)$$

where d_1 and d_2 refer to the two distorted images obtained by different synthesis methods and M, N are the width and height of the image.

3.3. Error prone area selection

Another option for selecting relevant spatial locations that need to be evaluated when comparing synthesis methods, is to look directly at the differences between methods. We can select these areas by generating a new selection mask containing all areas which were rendered differently by the two methods as shown in Eq. 9:

$$B_{epas}(x,y) = \begin{cases} 0 & \text{if } \mid (I_{d_1}(x,y) - I_{d_2}(x,y)) \mid < \mathcal{T} \\ 1 & \text{if } \mid (I_{d_1}(x,y) - I_{d_2}(x,y)) \mid \geq \mathcal{T} \end{cases} \quad (9)$$

where $(\mathcal{T})$ is a threshold.

When comparing two synthesis methods, we are interested to see their behavior in areas where pixels are predicted differently. Evaluating areas where both methods provide similar pixel predictions will not offer a good comparison of the methods. Establishing a selection threshold in this case is easier. Since we are interested in relative large differences, the mean absolute error can provide a good threshold.

4. EXPERIMENTAL RESULTS

In order to verify our evaluation method we use the 3D-HEVC test model (3D-HTM). The encoder and renderer configurations follow the Common Test Conditions (CTCs) for conducting experiments with 3D-HEVC, more details can be found here [29]. The tested video sequences are: Balloons, Kendo, NewspaperCC and PoznanHall2. The first three sequences have a resolution of 1024×768 with 30 fps and a total of 300 frames. The later has a resolution of 1920×1088 with 25 fps and a total of 200 frames. For each sequence, we use two encoded reference views with their associated depth maps and synthesize an intermediate view. For Balloons and Kendo sequences, we use views $1\&5$ as reference and synthesize view 3. Views $2\&6$ and $5\&7$ are used as reference for NewspaperCC and PoznanHall2 sequences respectively, while views 4 and 6 are synthesized. The encoding is performed with 3D-HEVC using four QPs for texture: 25, 30, 35, 40. Different QPs are used for the depth maps, as recommended by the CTCs: 34, 39, 42, 45.

The synthesis methods we evaluate are detailed in Sec. 2. For VSRS-1DFast we use the CTCs recommended configuration. The similarity enhancement and sub pixel precision options are active. The warping and filtering technique (Wf) presented in [26] uses a filtering window of size 7 and a sub pixel precision factor of $1/4$. The method based on temporal and inter-view prediction blending (P+Badapt) in [28] uses an optical flow implementation for motion estimation [30] and a temporal prediction distance of two. Each method is evaluated using PSNR and MSSIM. SSIM_{hist} and SSIM_{epas} are used to evaluate and compare Wf and P+Badapt with VSRS-1DFast.

Table 1 shows the PSNR results for the three tested methods: VSRS-1DFast, Wf and P+Badapt. On the bottom of the table we can see the average result across sequences and the last row shows the gain obtained by the later two methods. As can be seen both Wf and P+Badapt out perform VSRS-1DFast while the best results are obtained by P+Badapt. Another aspect of interest is that the gain remains relatively sta-

Table 1. Average PSNR for all tested methods and sequences at each QP.

Sequence	VSRS-1DFast PSNR (dB)				Wf PSNR (dB)				P+Badapt PSNR (dB)			
QPs	25	30	35	40	25	30	35	40	25	30	35	40
Balloons	34.37	34.07	33.43	32.41	34.39	34.14	33.52	32.51	34.74	34.45	33.8	32.72
Kendo	34.98	34.51	33.77	32.75	35.37	34.9	34.15	33.08	35.37	34.87	34.13	33.06
NewspaperCC	29.2	29.05	28.78	28.31	29.81	29.69	29.39	28.83	29.85	29.74	29.44	28.9
PoznanHall2	36.24	35.87	35.36	34.55	36.35	36.02	35.51	34.77	36.49	36.2	35.7	34.86
Average	33.70	33.37	32.83	32	33.98	33.69	33.14	32.3	34.11	33.82	33.27	32.38
ΔPSNR	-	-	-	-	**0.28**	**0.32**	**0.31**	**0.3**	**0.41**	**0.45**	**0.44**	**0.38**

Table 2. Average MSSIM for all tested methods and sequences at each QP.

Sequence	VSRS-1DFast MSSIM				Wf MSSIM				P+Badapt MSSIM			
QPs	25	30	35	40	25	30	35	40	25	30	35	40
Balloons	.9583	.9541	.9460	.9322	.9571	.9530	.9450	.9313	.9597	.9556	.9479	.9343
Kendo	.9635	.9593	.9528	.9430	.9631	.9590	.9526	.9429	.9638	.9600	.9538	.9444
NewspaperCC	.8965	.8898	.8771	.8573	.9004	.8939	.8802	.8590	.9020	.8957	.8824	.8621
PoznanHall2	.9352	.9322	.9272	.9190	.9358	.9330	.9281	.9198	.9370	.9340	.9290	.9208
Average	.9384	.9339	.9258	.9129	.9391	.9347	.9265	.9133	.9406	.9363	.9283	.9154
Δ MSSIM	-	-	-	-	**.0007**	**.0009**	**.0007**	**.0004**	**.0022**	**.0025**	**.0025**	**.0025**

Table 3. VSRS-1DFast and Wf evaluation for all QPs with SSIM_{hist} and SSIM_{epas}.

Sequence	VSRS-1DFast								Wf							
QPs	25		30		35		40		25		30		35		40	
Method	hist	epas	hist	epas	hist	epas	hist	epas	hist	epas	hist	epas	hist	epas	hist	epas
Balloons	.8546	.9186	.8550	.9120	.8593	.8970	.8396	.8708	.8464	.9112	.8473	.9052	.8535	.8905	.8356	.8649
Kendo	.8798	.9279	.8743	.9192	.8613	.9058	0.8407	.8852	.8717	.9239	.8678	.9149	.8568	.9019	.8375	.8819
NewspaperCC	.6062	.8309	.5592	.8173	.5958	.8050	.5763	.7801	.6194	.8358	.5753	.8243	.6078	.8113	.5866	.7841
PoznanHall2	.7517	.8922	.7359	.8834	.7254	.8699	.7041	.8485	.7466	.8932	.7345	.8857	.7300	.8739	.7095	.8527
Average	.7731	.8924	.7561	.8830	.7605	.8694	.7402	.8462	.7710	.8910	.7562	.8825	.7621	.8694	.7423	.8459
Δ	-	-	-	-	-	-	-	-	**-.0021**	**-.0014**	**.0001**	**-.0004**	**.0016**	**0**	**.0021**	**-.0002**

Table 4. VSRS-1DFast and P+Badapt evaluation for all QPs with SSIM_{hist} and SSIM_{epas}.

Sequence	VSRS-1DFast								P+Badapt							
QPs	25		30		35		40		25		30		35		40	
Method	hist	epas	hist	epas	hist	epas	hist	epas	hist	epas	hist	epas	hist	epas	hist	epas
Balloons	.8615	.9138	.8585	.9080	.8624	.8943	.8415	.8697	.8702	.9195	.8667	.9138	.8692	.9008	.8480	.8771
Kendo	.8844	.9238	.8779	.9159	.8611	.9035	.8423	.8842	.8789	.9237	.8743	.9166	.8583	.9055	.8402	.8879
NewspaperCC	.6073	.8265	.5514	.8121	.5876	.7996	.5955	.7749	.6245	.8366	.5735	.8254	.6062	.8134	.6143	.7891
PoznanHall2	.7494	.9077	.7312	.9034	.7230	.8967	.7023	.8812	.7630	.9122	.7478	.9087	.7389	.9021	.7163	.8876
Average	.7756	.8929	.7548	.8849	.7585	.8735	.7454	.8525	.7842	.8980	.7656	.8911	.7682	.8805	.7547	.8604
Δ	-	-	-	-	-	-	-	-	**.0085**	**.0051**	**.0108**	**.0063**	**.0096**	**.0069**	**.0093**	**.0079**

ble across QPs. Using the MSSIM metric shows similar results, as can be observed in Table 2.

Table 4 shows the results obtained when evaluating Wf against VSRS-1DFast with the proposed methods: SSIM_{hist}, SSIM_{epas}. We can see that losses or gains are slightly increased and better differentiated in comparison to MSSIM results. Also, when computing the difference between the average values we no longer have a gain at low QPs. This indicates that while the Wf method improves the overall image in comparison to VSRS-1DFast, it does not provide any benefits toward reducing the object boundary distorsions. The PSNR and MSSIM gains provided by this method are given by a reduction in small errors. This is expected since the method proposes a sub-pixel precision warping technique with high accuracy, without tackling the structural aspect of the scene.

The comparison results of P+Badapt and VSRS-1DFast are reported in Table 4. A significant increase in Δ values can be observed in comparison to MSSIM. SSIM_{hist} focuses on high synthesis errors which are most likely caused by object boundary distortions, as discussed in Section 1. We can conclude that P+Badapt improves the synthesis from a structural point of view. This is also visible in Fig. 3, where P+Badapt shows noticeable improvements on object edges.

Another interesting aspect is the behavior of ΔSSIM_{hist}

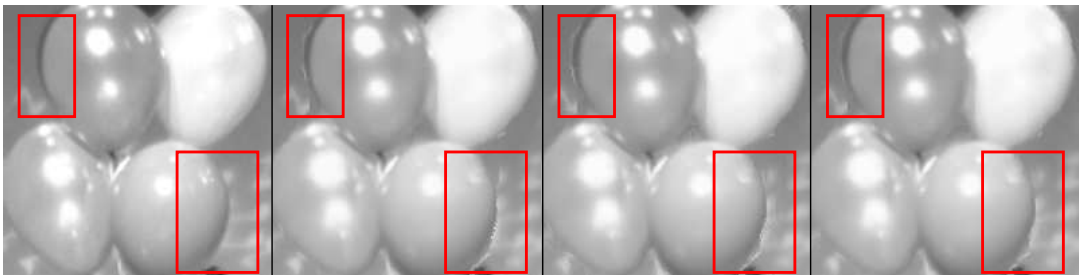

(a) Balloons

(b) NewspaperCC

Fig. 3. Details in Balloons 3(a) and NewspaperCC 3(b) sequences on frame 38. From left to right: original uncompressed, VSRS-1DFast, Wf, P+Badapt.

and ΔSSIM$_{epas}$ across QPs. While the ΔMSSIM and ΔPSNR report similar values across QPs, we can see that in Table 3 SSIM$_{hist}$ has a tendency to increase at lower QPs. This behavior can be explained by the threshold selection process described in 3.2. As the QP increases the quantization errors are in turn increased and they become closer to the high synthesis errors. Thus, the evaluated areas may contain more artifacts caused by quantization, reflecting the better overall warping precision of Wf over VSRS-1DFast and masking the structural distortions. However, definitive conclusions should be drawn from a more thorough evaluation of SSIM$_{hist}$ and SSIM$_{epas}$, using smaller QP steps.

Furthermore, in Fig. 4(a) we show the behavior over time of MSSIM and our proposed evaluation technique. While MSSIM score is relatively similar across frames, variations can be observed for SSIM$_{hist}$ and SSIM$_{epas}$ scores. Additional information about a methods strengths or weaknesses can be extrapolated from analyzing these variations. Let us look for example at three time instances marked in Fig. 4(a) with vertical red lines (t_1, t_2 and t_3, frames 40, 58 and 85 respectively). We can clearly notice an increase in SSIM$_{epas}$ at t_2 in comparison to t_1. This is consistent with MSSIM, however, it is hardly noticeable. Let us look at the SSIM$_{epas}$ masks for the two time instances in Fig. 4(b) and 4(c) to identify the cause. We can see the error prone area marked with a red square in Fig. 4(b). In Fig. 4(c) this area is obstructed by a person walking in front of it and the errors are concealed. Also, observe that ΔSSIM$_{epas}$ is smaller between frames 50 and 70. This points to Wf method achieving higher quality than VSRS-1DFast in this area. Obviously when the area is obstructed the gain is reduced.

At t_3 we can see a sudden drop in SSIM$_{epas}$ which is not viewable in MSSIM. Looking at the selection mask we can observe the person approaching another foreground object which is identified as an error prone area by the selection mask. This is marked with a red square in Fig. 4(d). To better understand why we have quality loss on this frame, let us look at the texture. In Fig. 4(e) we can see the reference frame and the VSRS-1dFast and Wf synthesized frames respectively. It is easily noticeable that both methods will have new artifacts in this area at t_3. This type of artifact appears due to the proximity of the two objects in the foreground. The area in-between them is not visible in the left or right base views (i.e. disoccluded area). This additional information on the tested methods, in terms of structural configuration of the scene and error prone areas, cannot be easily extrapolated by using only MSSIM or PSNR.

5. CONCLUSIONS

In this paper, we presented a distortion evaluation technique for view synthesis methods based on the SSIM metric. We compute the SSIM index on areas which are prone to synthesis errors such as object boundaries and complex textures. The area selection is performed either through a separation between structural artifacts caused by synthesis and quantization errors from the encoding process of left and right base views, or by directly selecting areas which are predicted differently by two evaluated synthesis methods. The evaluation was performed on three view synthesis methods and four multiview sequences, using 3D-HEVC encoding at four QPs 25, 30, 35 and 40, against PSNR and SSIM results. The proposed technique is shown to provide a better differentiation between

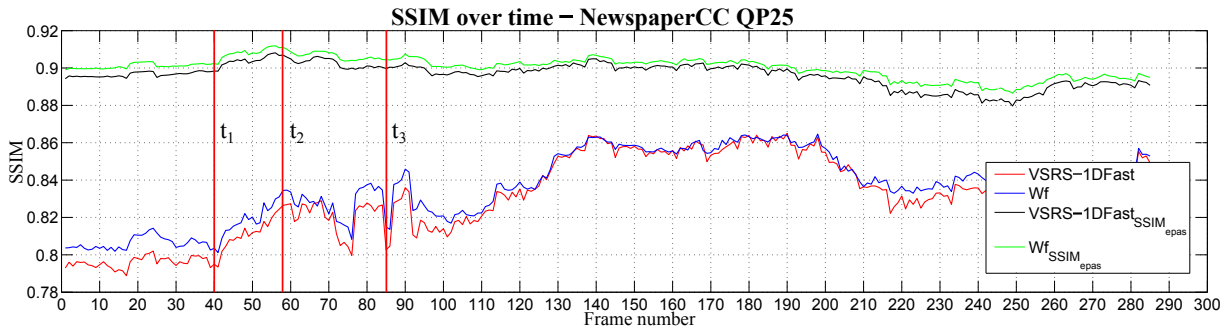

(a) NewspaperCC, $MSSIM$ and SSIM$_{epas}$ for VSRS-1DFast & Wf

(b) NewspaperCC, SSIM$_{epas}mask, frame40$ (c) NewspaperCC, SSIM$_{epas}mask, frame58$ (d) NewspaperCC, SSIM$_{epas}$ mask, frame 85

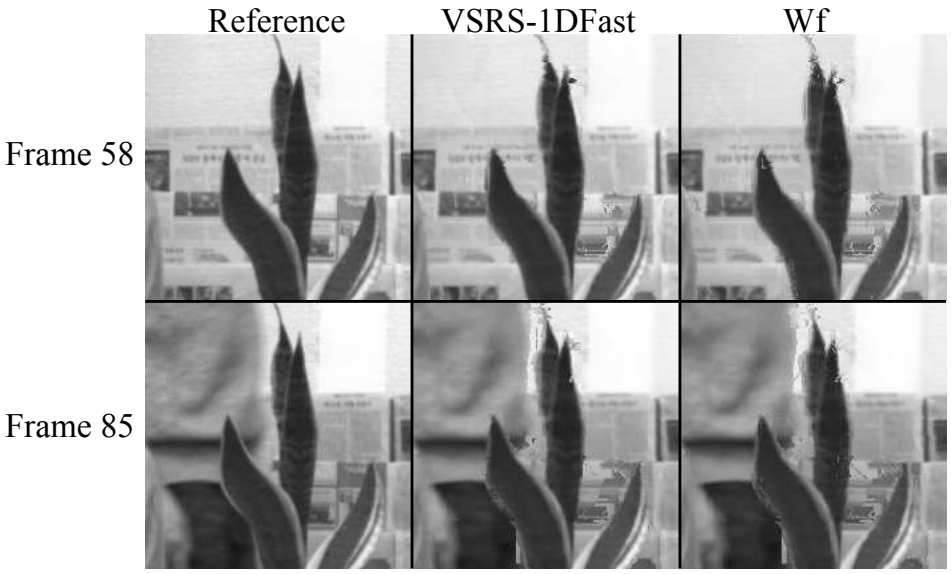

(e) NewspaperCC details

Fig. 4. Figure 4(a) - SSIM and SSIM$_{epas}$ over time. Figures 4(b), 4(c) and 4(d) show the selection masks for SSIM$_{epas}$. Figure 4(e) shows details of NewspaperCC sequence.

synthesis methods. Also, additional information can be extrapolated about the scene structure and spatial positioning of artifacts, while providing a good indication of the impact of synthesis errors.

6. REFERENCES

[1] M. Tanimoto, M. P. Tehrani, T. Fujii, and T. Yendo, "Free-Viewpoint TV," *IEEE Signal Processing Magazine*, vol. 28, pp. 67–76, 2011.

[2] F. Dufaux, B. Pesquet-Popescu, and M. Cagnazzo, Eds., *Emerging technologies for 3D video: content creation, coding, transmission and rendering*. Wiley, May 2013.

[3] P. Merkle, A. Smolic, K. Muller, and T. Wiegand, "Multi-view video plus depth representation and coding," *IEEE International Conference on Image Processing*, vol. 1, pp. 201–204, 2007.

[4] C. Fehn, "A 3D-TV approach using depth-image-based rendering," in *3rd IASTED Conference on Visualization, Imaging, and Image Processing*, Benalmadena, Spain,

8-10 September 2003, pp. 482–487.

[5] H. Shum and S. B. Kang, "Review of image-based rendering techniques," *SPIE Visual Communications and Image Processing*, vol. 4067, pp. 2–13, 2000. [Online]. Available: http://dx.doi.org/10.1117/12.386541

[6] L. Zhan-Wei, A. Ping, L. Su-xing, and Z. Zhao-yang, "Arbitrary view generation based on DIBR," in *International Symposium on Intelligent Signal Processing and Communication Systems (ISPACS)*, Xiamen, People's Republic of China, 2007, pp. 168–171.

[7] C.-M. Cheng, S.-J. Lin, S.-H. Lai, and J.-C. Yang, "Improved novel view synthesis from depth image with large baseline," in *19th International Conference on Pattern Recognition (ICPR)*, 2008, pp. 1–4.

[8] F. Dufaux, M. Cagnazzo, and B. Pesquet-Popescu, *Motion Estimation - a Video Coding Viewpoint*, ser. Academic Press Library in Signal Processing, R. Chellappa and S. Theodoridis, Eds. Academic Press, 2014 (to be published), vol. 5: Image and Video Compression and Multimedia.

[9] R. Krishnamurthy, P. Moulin, and J. Woods, "Optical flow techniques applied to video coding," in *IEEE International Conference on Image Processing (ICIP)*, vol. 1, 1995, pp. 570–573 vol.1.

[10] M. Levoy and P. Hanrahan, "Light field rendering," in *Proceedings of SIGGRAPH*, ser. SIGGRAPH '96. New York, NY, USA: ACM, 1996, pp. 31–42. [Online]. Available: http://doi.acm.org/10.1145/237170.237199

[11] H.-Y. Shum and L.-W. He, "Rendering with concentric mosaics," in *Proceedings SIGGRAPH*, Los Angeles, California USA, 1999, pp. 299–306.

[12] C. Buehler, M. Bosse, L. McMillan, and S. Gortler, "Unstructured Lumigraph Rendering," in *Proc SIGGRAPH*, Los Angeles, California USA, August 2001, pp. 425–432.

[13] "High Efficiency Video Coding," ITU-T Recommendation H.265 and ISO/IEC 23008-2 HEVC, April 2013.

[14] "Report on experimental framework for 3D video coding," ISO/IEC JTC1/SC29/WG11 MPEG2010/N11631, October 2010.

[15] L. Zhang, G. Tech, K. Wegner, and S. Yea, "3D-HEVC test model 5," ITU-T SG16 WP3 and ISO/IEC JTC1/SC29/WG11 JCT3V-E1005, July 2013.

[16] I. Daribo and B. Pesquet-Popescu, "Depth-aided image inpainting for novel view synthesis," in *IEEE MMSP*, Saint Malo, France, 4-6, October 2010.

[17] C. Guillemot and O. L. Meur, "Image inpainting: Overview and recent advances," *IEEE Signal Processing Magazine*, vol. 31, pp. 127–144, 2014.

[18] A. Criminisi, P. Perez, and K. Toyama, "Region filling and object removal by exemplar-based image inpainting," *IEEE Transactions on Image Processing*, vol. 13, no. 9, pp. 1200–1212, 2004.

[19] W. Sun, O. C. Au, L. Xu, Y. Li, and W. Hu, "Novel temporal domain hole filling based on background modeling for view synthesis," in *IEEE International on Image Processing (ICIP)*, Orlando, FL, 30 Sept. - 3 Oct. 2012, pp. 2721 – 2724.

[20] K. P. Kumar, S. Gupta, and K. S. Venkatesh, "Spatio-temporal multi-view synthesis for free viewpoint television," in *3DTV-Conference: The True Vision-Capture, Transmission and Display of 3D Video (3DTV-CON)*, Aberdeen, 7-8 October 2013, pp. 1 – 4.

[21] S. Shimizu and H. Kimata, "Improved view synthesis prediction using decoder-side motion derivation for multiview video coding," in *3DTV-Conference: The True Vision - Capture, Transmission and Display of 3D Video (3DTV-CON)*, 2010, pp. 1–4.

[22] K.-Y. Chen, P.-K. Tsung, P.-C. Lin, H.-J. Yang, and L.-G. Chen, "Hybrid motion/depth-oriented inpainting for virtual view synthesis in multiview applications," *3DTV-CON*, pp. 1–4, 7-9 June 2010.

[23] S. Huq, A. Koschan, and M. Abidi, "Occlusion filling in stereo: theory and experiments," *Computer Vision and Image Understanding*, vol. 117, pp. 688–704, June 2013.

[24] P.-J. Lee and Effendi, "Adaptive edge-oriented depth image smoothing approach for depth image based rendering," in *IEEE International Symposium on Broadband Multimedia Systems and Broadcasting (BMSB)*, Shanghai, 24-26 March, 2010, pp. 1–5.

[25] Z. Wang and J. Zhou, "A novel approach for depth image based rendering, based on non-linear transformation of depth values," in *International Conference on Image Analysis and Signal Processing (IASP)*, Hubei, People's Republic of China, 21-23 October 2011, pp. 138–142.

[26] A. Purica, E. G. M., B. Pesquet-Popescu, M. Cagnazzo, and B. Ionescu, "Improved view synthesis by motion warping and temporal hole filling," in *ICASSP*. South Brisbane: IEEE, 19-24 April 2014, pp. 1191–1195.

[27] Z. Wang, A. C. Bovik, H. R. Sheikh, and E. P. Simoncelli, "Image quality assessment: From error visibility to structural similarity," *IEEE Transactions on Image Processing*, vol. 13, pp. 600–612, 2004.

[28] A. Purica, M. Cagnazzo, B. Pesquet-Popescu, F. Dufaux, and B. Ionescu, "View synthesis based on temporal prediction via warped motion vector fields," in *submitted ICASSP*. IEEE, March 2016.

[29] D. Rusanovsky, K. Muller, and A. Vetro, "Common Test Conditions of 3DV Core Experiments," ITU-T SG16 WP3 & ISO/IEC JTC1/SC29/WG11 JCT3V-D1100, April 2013.

[30] C. Liu. Optical flow Matlab/C++ code. http://people.csail.mit.edu/celiu/OpticalFlow/. [Online]. Available: http://people.csail.mit.edu/celiu/OpticalFlow/